Editors' Suggestion

Gigahertz-Clocked Teleportation of Time-Bin Qubits with a Quantum Dot in the Telecommunication *C* Band

M. Anderson,[1,2] T. Müller,[1,*] J. Skiba-Szymanska,[1] A. B. Krysa,[3] J. Huwer,[1] R. M. Stevenson,[1] J. Heffernan,[4] D. A. Ritchie,[2] and A. J. Shields[1]

[1] *Toshiba Research Europe Limited, 208 Science Park, Milton Road, Cambridge CB4 0GZ, United Kingdom*
[2] *Cavendish Laboratory, University of Cambridge, JJ Thomson Avenue, Cambridge CB3 0HE, United Kingdom*
[3] *EPSRC National Epitaxy Facility, University of Sheffield, Mappin Street, Sheffield S1 3JD, United Kingdom*
[4] *Department of Electronic and Electrical Engineering, University of Sheffield, 3 Solly Street, Sheffield S1 3JD, United Kingdom*

(Received 20 December 2019; accepted 30 March 2020; published 21 May 2020)

Teleportation is a fundamental concept of quantum mechanics with an important application in extending the range of quantum communication channels via quantum relay nodes. To be compatible with real-world technology such as secure quantum key distribution over fiber networks, such a relay node should ideally operate at gigahertz clock rates and accept time-bin-encoded qubits in the low-loss telecom band around 1550 nm. Here, we show that InAs-InP droplet-epitaxy quantum dots, with their sub-Poissonian emission near 1550 nm, are ideally suited for the realization of this technology. To create the necessary on-demand photon emission at gigahertz clock rates, we develop a flexible-pulsed optical-excitation scheme and demonstrate that the fast driving conditions are compatible with a low multiphoton emission rate. We show further that, even under these driving conditions, photon pairs obtained from the biexciton cascade show an entanglement fidelity close to 90%, comparable to the value obtained under continuous-wave excitation. Using asymmetric Mach-Zehnder interferometers and our photon source, we finally construct a time-bin qubit quantum relay able to receive and send time-bin-encoded photons and demonstrate mean teleportation fidelities of 0.82 ± 0.01, exceeding the classical limit by more than ten standard deviations.

DOI: 10.1103/PhysRevApplied.13.054052

I. INTRODUCTION

Quantum networks can enable quantum technologies ranging from secure communication to distributed quantum computation using quantum nodes at separate locations [1,2]. Semiconductor quantum dots (QDs) are promising candidates to realize a variety of these technologies, where their atomlike energy structure and spin-photon interface [3] facilitate the entanglement of separate spins for distributed quantum computing [4] or the generation of indistinguishable, ultrapure single photons [5,6] with strong polarization entanglement [7] for photonic quantum network applications. Much progress has been made recently in improving these photonic qualities to create near-ideal efficient on-demand single- and entangled photon sources [8–11], even outperforming weak Poissonian sources in terms of single-photon rates while avoiding the complications arising from multiphoton events [12,13].

When establishing larger-scale quantum networks over existing fiber infrastructure, attenuation and loss of the weak quantum signal due to photon absorption is a major challenge, limiting the achievable length of quantum network links. In contrast to classical signals, the no-cloning theorem prevents the simple amplification of quantum states, leading to the proposal of quantum repeater schemes instead [14]. A full quantum repeater requires either two-dimensional photonic graph states [15] or an operational quantum memory, practical demonstrations of which based on quantum dots are still outstanding despite recent progress in this direction [16,17]. However, it is already feasible to operate quantum relay nodes [18] to increase the signal-to-noise ratio over extended distances. There are many proof-of-principle demonstrations of this concept [19–22]; however, there are a few key differences in how QD technology and existing network applications such as quantum key distribution (QKD) are typically operated. These need to be overcome if practical integration of QD-based quantum relays with QKD systems is to be realized. They concern the operating wavelength,

*tina.muller@crl.toshiba.co.uk

operating frequency, and encoding scheme, all of which are addressed in this work.

For long-distance fiber quantum networks it is important to use the low-loss window in telecom fibers around 1550 nm (the *C* band) to maximize transmission of qubits. In contrast, the most mature QD devices operate at wavelengths around 900 nm. Encouragingly, there has been recent progress in developing low-strain InAs QD devices with an emission wavelength in the *C* band directly using two alternative approaches, one of which includes metamorphic buffers as relaxation layers in more traditional GaAs-based devices, while the other—the approach used here—consists in swapping the GaAs matrix material for InP. Both approaches have delivered single-photon emission [23–26] and small fine-structure splitting (FSS) [27,28], resulting in entangled photon emission [28,29]. However, compared to GaAs-based *C*-band devices [30], the coherence times are an order of magnitude closer to the Fourier limit for InP-based devices [31], which remain the system of choice when implementing interference-based applications such as quantum relays.

Further, QKD systems tend to use high clock rates of 1 GHz and above [32], while for QD systems, the clock rates under pulsed excitation are limited to the region of 80 MHz for *C*-band QDs and, even for lower-wavelength QDs, entangled photon pairs have not been generated at frequencies higher than 400 MHz [33].

Finally, long-distance QKD systems tend to use time-bin-encoded qubits to increase robustness [34,35] during long-distance fiber transmission. QDs, on the other hand, natively produce polarization-encoded single photons and entangled photons via the biexciton cascade. To overcome this incompatibility, schemes based on weak pulsed excitation have been developed to implement time-bin-encoded single photons [36] and entangled photon pairs [37–40] directly from quantum dots. Direct time-bin-encoded entanglement generation from quantum dots has the advantage that larger FSSs are acceptable [37] but this scheme cannot produce true on-demand entangled pairs without the addition of a metastable state [37, 38] and is technically demanding due to the need for phase control between the early and late photons, which can only be achieved with resonant two-photon excitation [39,40]. Alternatively, in the approach favored here, qubit transcoder setups using asymmetric Mach-Zehnder interferometers (AMZIs) can be used to create time-bin-entangled photons from polarization-entangled ones [41,42]; however, demonstrations of this principle using *C*-band QDs are still outstanding.

In this work, we simultaneously address the above three key challenges to create a gigahertz clock rate on-demand time-bin-compatible telecom-wavelength quantum relay integrable with existing QKD technology and suitable for use with a variety of long-distance quantum network applications. A conceptual overview of our relay node is shown in Fig. 1.

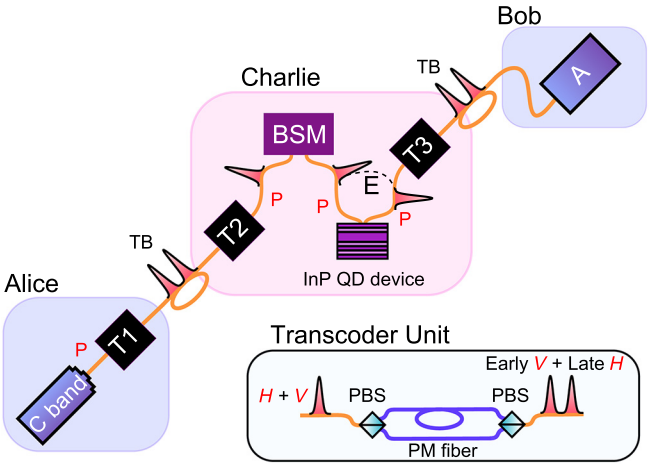

FIG. 1. Interfacing gigahertz-clocked time-bin qubits with a quantum-dot relay. Alice produces a gigahertz-clocked time-bin-encoded qubit by sending polarization-encoded weak coherent pulses through an interferometric transcoding unit. Subsequent time-encoded photons are then sent to a relay node, Charlie, where upon conversion back into polarization encoding using a phase-stabilized second transcoding unit, the state can be teleported using a gigahertz-clocked polarization-entangled photon-pair source. After successful teleportation at Charlie, photons can again be transcoded to time-bin encoding before being sent on to a receiver, Bob. P, polarization qubit; TB, time-bin qubit; T1–T3, transcoder units; A, time-bin qubit analysis; BSM, Bell-state measurement; E, entnalged photon pairs.

At the core of the relay station at Charlie is an InP-based InAs droplet-epitaxy QD device, which offers low FSS and emission near 1550 nm with a high degree of polarization entanglement [29] and long coherence times [31]. The QDs are optically driven at gigahertz clock rates using a flexible-pulse-generation setup developed in house. To interface the time-bin-entangled qubits at Charlie's input with the emitted polarization-entangled photon pairs, we construct a qubit transcoding unit based on stabilized AMZIs as described further below. Such a transcoder is also used to convert Charlie's output back to efficient time-bin encoding before being sent over a fiber link to Bob and to produce time-bin-encoded qubits at Alice to send to Charlie from gigahertz-clocked polarization-encoded pulses. In this manner, we are able to create and teleport arbitrary time-bin-encoded superpositions of the basis states.

The paper is organized as follows. We start by characterizing the QD emission under gigahertz-clocked pulsed optical excitation, measuring lifetimes and autocorrelations to reveal the absence of multiple photons in the same emission cycle. We then measure the entanglement fidelity achieved under these driving conditions using full tomography and compare it to the entanglement fidelity obtained

under continuous-wave (cw) and low-repetition-rate (100-MHz) excitation. Next, we characterize the teleportation process with time-bin-encoded states in three independent bases, before demonstrating that a time-bin-encoded polar state is indeed mapped to the correct output time bin at Bob.

II. GIGAHERTZ-CLOCKED EMISSION

We begin by introducing our scheme for creating flexible excitation pulses using an electro-optic modulator (EOM), a pulse generator, and a dc offset to precisely control the pulse width, repetition rate, and background suppression of the pulses created. A schematic of the setup used is shown in Fig. 2(a), where a 1310-nm cw laser is sent through a 20-GHz bandwidth EOM and a polarizer for intensity modulation. A pulse generator is used to define narrow [full width at half maximum (FWHM) of 160 ps] excitation pulses. In order to maintain > 20 dB suppression of the laser between the excitation pulses, we measure the average beam intensity and use a feedback control loop to the dc offset of the EOM to keep it constant. The resulting excitation pulses are then passed through a fiber polarization controller (PC) and a digital variable attenuator (DVA) before being sent to the QD. With this setup, we are able to achieve a high level of control over the excitation conditions at various frequencies of interest.

To characterize the behavior of our source under pulsed excitation, we examine the time-resolved response of the QD. A spectrum of the selected QD emitting near the telecom C band when excited at a repetition rate of 1.07 GHz is shown in the inset to Fig. 2(a), in which several emission lines originating from different excitonic configurations can be seen. The lines of interest for this work are the neutral biexciton (XX) and exciton (X), which have been determined by polarization-resolved and intensity-correlation measurements and show count rates of 280 kcps and 90 kcps, respectively. The FSS is determined

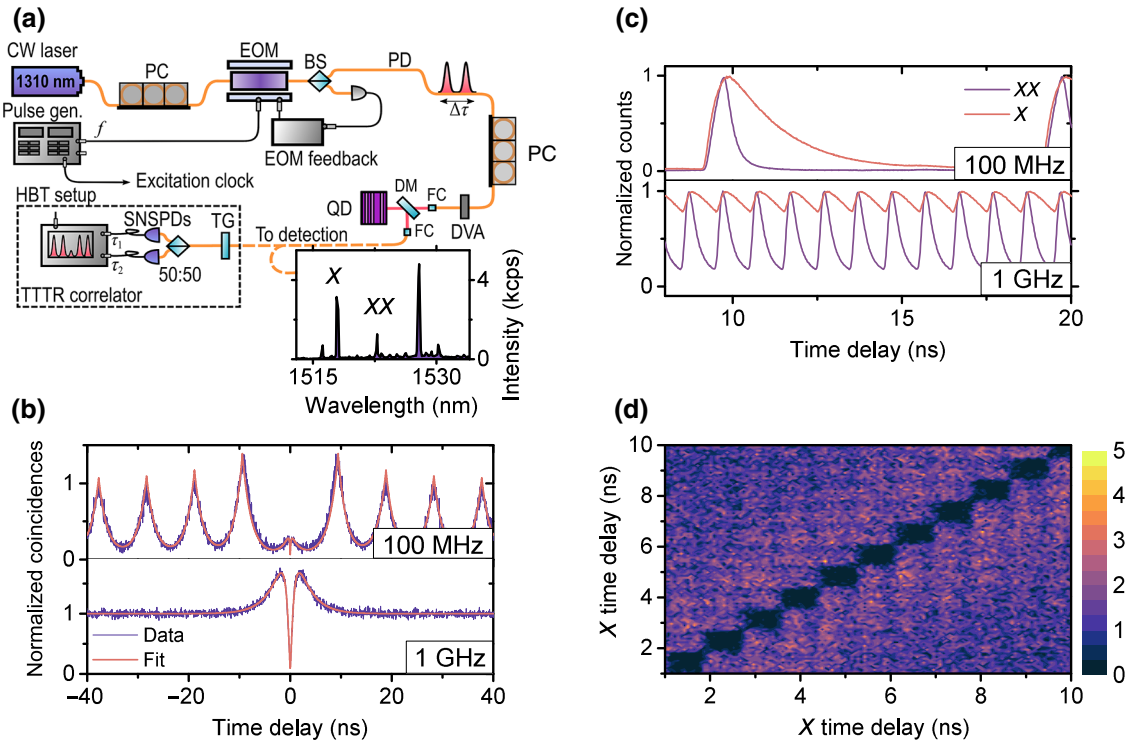

FIG. 2. The gigahertz-clocked emission from a QD emitting near the telecom C band. (a) A schematic of the excitation setup. A 1310-nm cw laser is modulated by an EOM with active voltage stabilization in order to create flexible excitation pulses. The gigahertz-clocked emission is collected from the QD and sent to the detection system, where time-resolved measurements can be made using the excitation clock from the pulse generator: PC, polarization controller; EOM, electro-optic modulator; BS, beam splitter; PD, photodiode; DM, dichroic mirror; FC, fiber coupler; DVA, digital variable attenuator; TG, transmission grating; SNSPDs, superconducting-nanowire single-photon detectors. The inset shows the spectrum of the QD measured under pulsed excitation at a power where the exciton intensity begins to saturate. The emission lines of the exciton (X) and the biexciton (XX) are labelled. (b) The second-order intensity correlations of the X for 100-MHz (top) and 1.07-GHz (bottom) excitation frequencies. The solid lines show fits to the data. (c) The time-resolved intensity of the X and the XX emission lines at a repetition frequency of 100 MHz (top) and 1.07 GHz (bottom). (d) The second-order correlation of the X photons, measured with respect to the excitation laser clock. The data binned on a 40×40 ps grid show a leading diagonal of empty photon counts corresponding to the low probability of finding two X photons emitted in the same clock cycle. The color bar denotes normalized coincidences.

to be 6.2 ± 0.1 μeV. We first measure the time-resolved intensity for a repetition rate of $f = 100$ MHz and compare it to the time-resolved intensity at $f = 1$ GHz. Both curves are shown in Fig. 2(c) for the X and XX transitions. The lifetime measurements show the expected behavior, with a sharp turn on and similar relatively short lifetimes of 272 ± 2 ps and 262 ± 6 ps for the XX at 100 MHz and 1 GHz, respectively, and a slower turn on due to filling effects and a longer lifetime of 1.56 ± 0.01 ns at both repetition rates for X. At a 100-MHz repetition rate, this leads to well-separated pulses of QD emission. For the above-gigahertz excitation rate common for many QKD protocols, however, the excitation period becomes comparable to the radiative lifetimes, reducing the on-off contrast of the resulting emission to around 12% for the X and 69% for the XX.

One might expect that the overlap of radiative decay cycles will affect the degree of multiphoton suppression under high-repetition-rate driving. Looking at the intensity autocorrelations using the Hanbury Brown–Twiss (HBT) setup shown in Fig. 2(a), in a standard histogram of the delays between photons, we find the expected pulse signature when driving at 100 MHz, as shown in Fig. 2(d), where the finite intensity for the zero-delay pulse is mainly due to reexcitation effects. For a 1-GHz repetition rate, however, we see a strong cw-like signature, including bunching wings around the zero-delay dip. Interestingly though, when comparing the excitation repetition rates of 100 MHz and 1 GHz, we find that the degree of multiphoton suppression is comparable, with $g^{(2)}(0)$ values of 0.14 ± 0.01 and 0.09 ± 0.05, respectively, determined by fits to the experimental data. In both cases, the $g^{(2)}(0)$ is far below the 0.5 threshold required to prove predominant emission into the single-photon Fock state. For the 100-MHz data, the model includes the effects from both a shelving state (increased probability for time delays $> |\tau_0|$) and reexcitation (small volcanolike feature around the zero delay [43]). For the 1.07-GHz measurement, a standard multilevel cw model is used.

To recover the signature of true on-demand pulsed single-photon emission even at gigahertz-clock-rate driving conditions, we measure the arrival times of both X photons in the HBT setup with respect to a common clock. The result of this measurement can be seen in Fig. 2(e). Remarkably, we find that along the diagonal, corresponding to zero-delay coincidences of both X detectors, there is an absence of photons within the same 0.935×0.935 ns square determined by the 1.07-GHz repetition rate, with $g^{(2)}(0) = 0.33 \pm 0.01$. This shows clearly that there is a lack of multiphoton events within one entire excitation and emission period. Hence, despite the long radiative lifetime of this QD, we are able to generate single-photon emission clocked at 1 GHz.

The next consideration when preparing for pulsed teleportation is to look at the effect of the pulse repetition rate on the entanglement generated by the XX-X cascaded emission. In this process, after excitation of the XX, subsequent radiative recombination to the intermediate X state and then to the ground state results in a polarization-entangled two-photon state of the form

$$|\Psi(\tau)\rangle = \frac{1}{\sqrt{2}}\left[|H_{XX}H_X\rangle + e^{i\Delta E\tau/\hbar}|V_{XX}V_X\rangle\right], \quad (1)$$

where ΔE is the FSS. In the limit of vanishing FSS, the state is no longer time evolving and has the form of the symmetric $|\Phi^+\rangle$ Bell state. For excitation at 1 GHz, we fully characterize this state via quantum state tomography [44,45] to reconstruct the two-photon density matrix (ρ) from a complete set of XX-X polarization cross-correlations measured in three mutually unbiased bases. We utilize the maximum-likelihood approach [45] in the reconstruction to ensure that the resulting matrix is Hermitian and positive semidefinite. The resulting density matrix expressed in the QD eigenbasis is shown in Fig. 3(a) for a 96-ps window around the zero delay and has a strong fidelity to the $|\Phi^+\rangle$ Bell state of 0.88 ± 0.01. The second-strongest contribution, at 0.04, are classical correlations between H and V where the phase information has been lost. These are most likely a consequence of the finite timing resolution of our detectors (approximately 100 ps). Further deviations of the matrix away from the ideal Bell

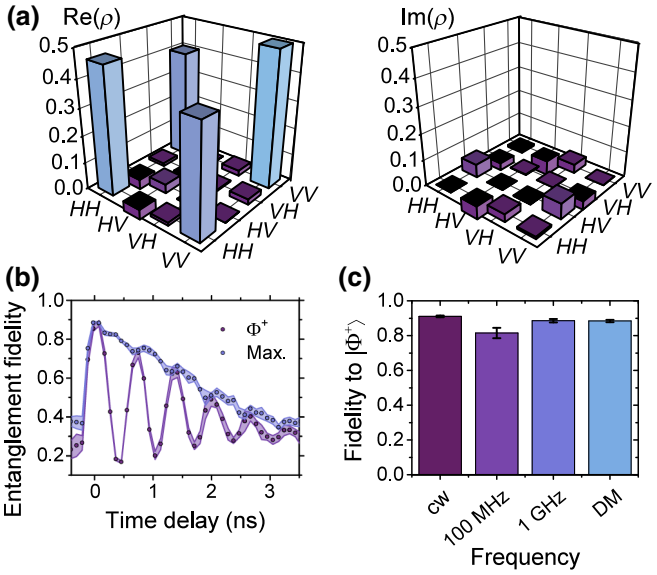

FIG. 3. The degree of entanglement under gigahertz-clocked excitation. (a) The real (left) and imaginary (right) parts of the two-photon density matrix, reconstructed using a time window of 96 ps, under pulsed optical excitation clocked at 1.07 GHz. (b) The evolution of the fidelity of the two-photon state to the Φ^+ Bell state and a maximally entangled state, calculated from the two-photon density matrix for different 96-ps time windows. (c) A comparison of the maximum fidelity to the Φ^+ Bell state for different driving frequencies (see text for details).

state can be attributed to experimental imperfections as well as contributions from uncorrelated emission from the sample. From the density matrix, we can also evaluate the concurrence, with the maximum determined here to be 0.80 ± 0.01.

As a result of the FSS, a time-dependent phase is accrued during the time spent in the intermediate X state, as described in Eq. (1). Thus, the expected fidelity to the Bell state oscillates at a beat frequency proportional to the magnitude of the FSS. We evaluate the fidelity of the reconstructed matrix for multiple time windows of 96 ps in order to reveal these quantum oscillations. The resulting fidelity is plotted in Fig. 3(b) alongside the fidelity to a maximally entangled state, which follows the fidelity to the time-evolving state of Eq. (1) that is usually displayed in our work [29].

The entanglement fidelities for the different driving frequencies considered here are compared in Fig. 3(c). We see that the values extracted from the reconstructed density matrix compare very well to those achieved under cw excitation (0.91 ± 0.01), 100 MHz (0.82 ± 0.03), and 1 GHz (0.89 ± 0.01) measured applying the approach previously used in our work [29], where the latter agrees perfectly with the value extracted from the density matrix (shown for completeness). Furthermore, for a gate width corresponding to one excitation period when clocked at 1.07 GHz, we determine a counts-weighted fidelity average of 0.81 ± 0.004 to a maximally entangled state with a detected entangled-pair rate of 32 ± 0.2 pairs per second into this gate. We expect this rate to increase significantly with further improvements to the structure and photonic engineering [9,10].

III. TIME-BIN-ENCODED QUANTUM RELAY

With the gigahertz-clocked emission and entanglement generation characterized, we proceed by performing teleportation of time-bin qubits. For the generation of the input qubits at Alice, we use a similar setup to that described in Fig. 2(a), where a feedback-controlled EOM is used to create gigahertz-clocked pulses with a width of 130 ps (FWHM) from a tuneable telecom C-band cw laser. These pulses are then encoded using a qubit transcoder (as described in Fig. 1), before being sent to the relay station at Charlie. In this way, logical time-bin-encoded states are created by mapping V-polarized photons onto the early time bin and H-polarized photons onto the late time bin. A phase can then be encoded between the early and the late pulses by fine tuning the delay between the two arms in order to create superposition-basis states. Examples of the

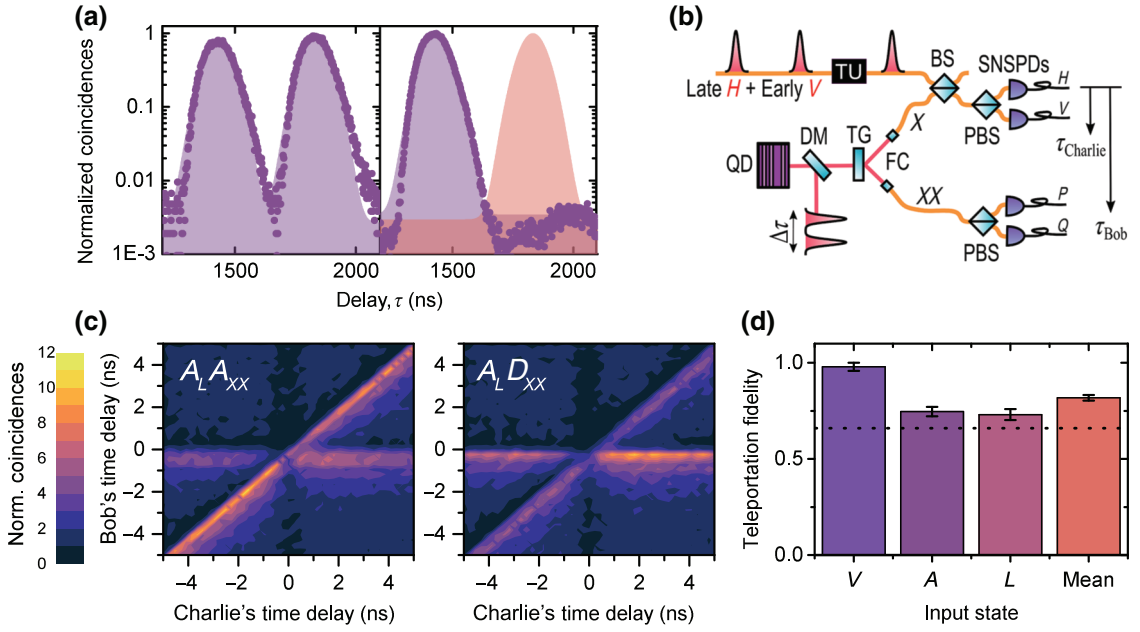

FIG. 4. Superposition-basis teleportation at 1 GHz. (a) Input laser qubits in the time-bin basis for a superposition state (left) and an early state (right). (b) A schematic of the polarization-basis relay station where a time-bin input laser qubit is sent through a transcoder unit (TU) before being teleported using an entangled photon pair generated from the QD. Other optical elements are as defined in Fig. 2. (c) The normalized third-order correlations for sending input laser qubits in a superposition of $|e\rangle$ and $|l\rangle$ time bins, which is subsequently mapped to an $|A\rangle$-polarized photon, and measuring $|A\rangle$- (left) and $|D\rangle$- (right) polarized photons at Bob. (d) The teleportation fidelities for a complete set of orthogonal input states, calculated from the third-order correlations centered on the time $t_{\mathrm{Bob}} = t_{\mathrm{Charlie}} = 0$, the point at which all three photons are measured simultaneously. The results for the most statistically significant equivalent postselection window size of 228 ps are shown. Each state surpasses the classical threshold of 2/3 and a mean fidelity of 0.82 ± 0.01 beats this limit by more than $10\,\sigma$.

simulated laser input states are shown in Fig. 4(a) for both a superposition-basis state and an early logical state. To interface these qubits with the QD polarization relay station at Charlie, a phase-matched decoding interferometer is used to map the states back into polarization, allowing the teleportation to proceed. The setup we use for the teleportation is similar to that described in our previous work [31] and the main experimental features are shown in Fig. 4(b) for clarity. An input qubit containing the polarization-encoded information to be teleported is incident upon a beam splitter together with the X photon from the QD entangled photon pair. When the photons arriving at the beam splitter are indistinguishable, they will exit through the same port as a result of the Hong-Ou-Mandel (HOM) interference effect. A polarizing beam splitter (PBS) placed after the interfering beam splitter is then used to perform a Bell-state measurement (BSM), which heralds the teleportation of the quantum state to the XX photon, measured at a second PBS.

In order to characterize the teleportation, we measure the triple coincidences HVP and HVQ, corresponding to the successful detection of the BSM at Charlie, and a P- or Q-polarized photon at Bob, respectively. An example of such a third-order correlation is shown in Fig. 4(c) for the case of teleporting a superposition-basis state. Here, the input laser is prepared in an equal superposition of $|e\rangle$ and $|l\rangle$. This state is then decoded into polarization and aligned to the QD $|A\rangle$ state. Three-photon coincidences HVA and HVD are then measured where, due to the experimental setup, the effect of this teleportation protocol is to map an $|A\rangle$ input to an $|A\rangle$ output at Bob. The peak in triple coincidences at $t_{\mathrm{Bob}} = t_{\mathrm{Charlie}} = 0$ is therefore expected to be seen when examining the HVA correlation and this is indeed the case, as shown in Fig. 4(c). Conversely, we see that there is an absence of three-photon events when looking at HVD correlations, corresponding to a teleportation fidelity $f_A^T = g_A^{(3)}(0)/[g_A^{(3)}(0) + g_D^{(3)}(0)]$ of 0.75 ± 0.03 for the most significant postselection window size of 228 ps. Measurement of at least three mutually orthogonal input states is required in order to prove the quantum nature of the teleportation [46] and so we measure the relevant correlations for the logical state $|e\rangle$, subsequently mapped to $|V\rangle$, as well as another equal-superposition state subsequently mapped to $|L\rangle$. The resulting fidelities are shown in Fig. 4(d), where we achieve a mean teleportation fidelity of 0.82 ± 0.01, more than 10 σ beyond the classical limit of $2/3$. At the expense of teleported photons, a maximum mean fidelity of 0.92 ± 0.04 can be achieved for a much smaller postselection window of 85 ps. These fidelities are comparable to those reached for teleportation of polarization qubits [31], proving the accuracy and stability of the time-bin-to-polarization-conversion interferometers.

We note that time gating is routinely employed in QKD experiments operating at such frequencies and, indeed, this time gating and the resultant avoidance of detector dark counts when no teleported photons are expected are responsible for the favorable scaling of the signal-to-noise ratio with distance for a quantum relay compared to direct transmission [18]. Of course, a reduction of both the radiative lifetime and the FSS of our dots would result in more photons of higher fidelity within the time window and thus would improve the efficiency of the quantum relay, while relaxing the requirements of the exact width of the gate used.

It is straightforward to now show that we can also convert the teleported photon back to time-bin encoding at Charlie before sending it to Bob. As a proof of principle, we teleport logical-basis states, $|e\rangle$ and $|l\rangle$, except that this time the output photon is then encoded back into the time-bin frame using a duplicate qubit transcoder. We implement this by sending Bob's photon back through the decoding interferometer, which guarantees a stable delay between early and late pulses for the two interferometers.

To determine that the output photon has been successfully teleported, we measure three-photon coincidences correlating a successful BSM in the polarization basis with the time-bin arrival of the XX photons, for a given time-bin input laser qubit $|e\rangle$ or $|l\rangle$. First, we consider the case when teleporting the $|e\rangle$ input laser qubit. Given that after qubit transcoding, the teleporter will map H-polarized photons to V and vice versa, we expect that the teleporter will map the early-input photons to late-output photons. Indeed, this can be seen in Fig. 5(a), where we

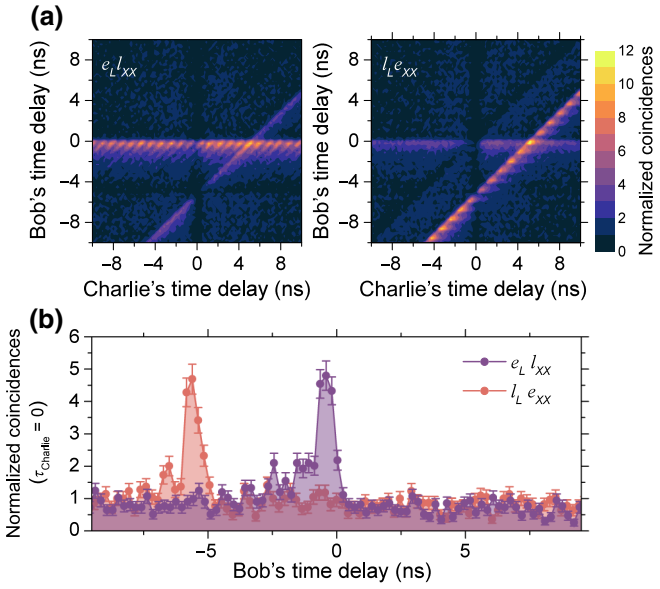

FIG. 5. Time-bin logical-basis teleportation. (a) The normalized third-order correlations for sending input laser qubits in $|e\rangle$ and $|l\rangle$ time bins, which are subsequently mapped to $|l\rangle$ and $|e\rangle$ time bins after sending Bob's photons back through the interferometer. (b) The teleportation fidelities along $t_{\mathrm{Charlie}} = 0$, showing that input $|e\rangle$ is mapped to $|l\rangle$, corresponding to the polarization mapping of $|H\rangle$ to $|V\rangle$ in the teleportation.

see a peak of coincidences at the time $t_{\mathrm{Bob}} = t_{\mathrm{Charlie}} = 0$ and an absence at $t_{\mathrm{Bob}} = -5$ ns along the $t_{\mathrm{Charlie}} = 0$ axis, confirming that Bob's photon went through the long arm of the conversion interferometer. The other characteristic feature of these plots is the absence of coincidences along the $t_{\mathrm{Bob}} = t_{\mathrm{Charlie}}$ axis, corresponding to simultaneous measurement of the laser/X and XX photons. These events have also been shifted by 5 ns to $t_{\mathrm{Bob}} = t_{\mathrm{Charlie}} - 5$ ns, where we see peaks of coincidences at the 1.07-GHz frequency of the system clock. Similarly, when sending a late photon, the expected outcome is an early one, as confirmed in the right-hand plot of Fig. 5(b). Here, a distinct peak of coincidences is seen at $t_{\mathrm{Bob}} = t_{\mathrm{Charlie}} = -5$, which corresponds to a successful mapping of the late to early time bins. The arrival times of early- and late-teleported photons are highlighted in Fig. 5(b), where we plot a cut along the $t_{\mathrm{Charlie}} = 0$ axis. The peak and absence of photons in the correct time bins results in a postselected teleportation fidelity of 0.89 ± 0.04 for both logical time-bin-encoded input states. This fidelity is comparable to that reached without the time-bin conversion for Bob's photon, again confirming the accuracy of the conversion process.

IV. CONCLUSION

In conclusion, we successfully address three of the major hurdles for integrating quantum-dot devices with long-distance quantum networks. We show gigahertz-clocked emission from a QD emitting near the telecom C band while maintaining a single-photon purity of 0.91 ± 0.05 postselected and 0.67 ± 0.01 across the entire excitation cycle and recording the highest fidelity and concurrence of entanglement generated nonresonantly from the cascaded emission of the XX for this type of source. The gigahertz-clocked entangled photon-pair source is then used to interface with a time-bin-encoded laser qubit to perform a pulsed quantum relay at telecom wavelengths.

While even a very inefficient quantum relay can beat the signal-to-noise ratio of a direct quantum link at long enough distances [18], improvements to the photon extraction efficiency of our device would be desirable for practical applications. The inclusion of our device into recently demonstrated structures suitable for entangled photon extraction, such as a circular Bragg grating [9,11] or a broadband antenna [8], could boost the probability of extracting an entangled photon pair by 4 orders of magnitude. At the same time, such devices could lead to much shortened radiative lifetimes through Purcell enhancement of the emission [47], which would not only allow for even higher clock rates and shorter delays between the $|e\rangle$ and $|l\rangle$ but could also bring the emitted photons closer to the Fourier-transform limit [48] and relax time-gating or postselection criteria [22] for the quantum relay. We expect these straightforward improvements to lead to the realization of a true push-button quantum teleportation scheme that is easily integrable into existing quantum technology in the telecom C band.

ACKNOWLEDGMENTS

We acknowledge partial financial support from the Engineering and Physical Sciences Research Council and the United Kingdom's innovation agency, Innovate UK. M.A. gratefully acknowledges support from the Industrial CASE award funded by the EPSRC and Toshiba Research Europe Limited.

[1] E. Knill, R. Laflamme, and G. J. Milburn, A scheme for efficient quantum computation with linear optics, Nature **409**, 46 (2001).

[2] H. J. Kimble, The quantum Internet, Nature **453**, 1023 (2008).

[3] W. B. Gao, P. Fallahi, E. Togan, J. Miguel-Sanchez, and A. Imamoglu, Observation of entanglement between a quantum dot spin and a single photon, Nature **491**, 426 (2012).

[4] R. Stockill, M. J. Stanley, L. Huthmacher, E. Clarke, M. Hugues, A. J. Miller, C. Matthiesen, C. Le Gall, and M. Atatüre, Phase-Tuned Entangled State Generation between Distant Spin Qubits, Phys. Rev. Lett. **119**, 010503 (2017).

[5] N. Somaschi, V. Giesz, L. de Santis, J. C. Loredo, M. P. Almeida, G. Hornecker, S. L. Portalupi, T. Grange, C. Antón, J. Demory, C. Gómez, I. Sagnes, N. D. Lanzillotti-Kimura, A. Lemaítre, A. Auffeves, A. G. White, L. Lanco, and P. Senellart, Near-optimal single-photon sources in the solid state, Nat. Photonics **10**, 340 (2016).

[6] X. Ding, Y. He, Z.-C. Duan, N. Gregersen, M.-C. Chen, S. Unsleber, S. Maier, C. Schneider, M. Kamp, S. Höfling, C.-Y. Lu, and J.-W. Pan, On-Demand Single Photons with High Extraction Efficiency and Near-Unity Indistinguishability from a Resonantly Driven Quantum Dot in a Micropillar, Phys. Rev. Lett. **116**, 020401 (2016).

[7] D. Huber, M. Reindl, J. Aberl, A. Rastelli, and R. Trotta, Semiconductor quantum dots as an ideal source of polarization-entangled photon pairs on-demand: A review, J. Opt. **20**, 073002 (2018).

[8] Y. Chen, M. Zopf, R. Keil, F. Ding, and O. G. Schmidt, Highly-efficient extraction of entangled photons from quantum dots using a broadband optical antenna, Nat. Commun. **9**, 2994 (2018).

[9] J. Liu, R. Su, Y. Wei, B. Yao, S. F. C. da Silva, Y. Yu, J. Iles-Smith, K. Srinivasan, A. Rastelli, J. Li, and X. Wang, A solid-state source of strongly entangled photon pairs with high brightness and indistinguishability, Nat. Nanotechnol. **14**, 586 (2019).

[10] H. Wang, H. Hu, T.-H. Chung, J. Qin, X. Yang, J.-P. Li, R.-Z. Liu, H.-S. Zhong, Y.-M. He, X. Ding, Y.-H. Deng, Q. Dai, Y.-H. Huo, S. Höfling, C.-Y. Lu, and J.-W. Pan, On-Demand Semiconductor Source of Entangled Photons Which Simultaneously Has High Fidelity, Efficiency, and Indistinguishability, Phys. Rev. Lett. **122**, 113602 (2019).

[11] H. Wang *et al.*, Towards optimal single-photon sources from polarized microcavities, Nat. Photonics **13**, 770 (2019).

[12] J. C. Loredo, M. A. Broome, P. Hilaire, O. Gazzano, I. Sagnes, A. Lemaitre, M. P. Almeida, P. Senellart, and A. G. White, Boson Sampling with Single-Photon Fock States from a Bright Solid-State Source, Phys. Rev. Lett. **118**, 130503 (2017).

[13] Y. He *et al.*, Time-Bin-Encoded Boson Sampling with a Single-Photon Device, Phys. Rev. Lett. **118**, 190501 (2017).

[14] H.-J. Briegel, W. Dür, J. I. Cirac, and P. Zoller, Quantum Repeaters: The Role of Imperfect Local Operations in Quantum Communication, Phys. Rev. Lett. **81**, 5932 (1998).

[15] K. Azuma, K. Tamaki, and H.-K. Lo, All-photonic quantum repeaters, Nat. Commun. **6**, 6787 (2015).

[16] D. A. Gangloff, G. Éthier-Majcher, C. Lang, E. V. Denning, J. H. Bodey, D. M. Jackson, E. Clarke, M. Hugues, C. Le Gall, and M. Atatüre, Quantum interface of an electron and a nuclear ensemble, Science **364**, 62 (2019).

[17] E. V. Denning, D. A. Gangloff, M. Atatüre, J. Mørk, and C. Le Gall, Collective Quantum Memory Activated by a Driven Central Spin, Phys. Rev. Lett. **123**, 140502 (2019).

[18] B. C. Jacobs, T. B. Pittman, and J. D. Franson, Quantum relays and noise suppression using linear optics, Phys. Rev. A **66**, 052307 (2002).

[19] J. Nilsson, R. M. Stevenson, K. H. A. Chan, J. Skiba-Szymanska, M. Lucamarini, M. B. Ward, A. J. Bennett, C. L. Salter, I. Farrer, D. A. Ritchie, and A. J. Shields, Quantum teleportation using a light-emitting diode, Nat. Photonics **7**, 311 (2013).

[20] C. Varnava, R. M. Stevenson, J. Nilsson, J. Skiba-Szymanska, B. Dzurňák, M. Lucamarini, R. V. Penty, I. Farrer, D. A. Ritchie, and A. J. Shields, An entangled-LED-driven quantum relay over 1 km, npj Quantum Inf. **2**, 145 (2016).

[21] J. Huwer, R. M. Stevenson, J. Skiba-Szymanska, M. B. Ward, A. J. Shields, M. Felle, I. Farrer, D. A. Ritchie, and R. V. Penty, Quantum-Dot-Based Telecommunication-Wavelength Quantum Relay, Phys. Rev. Appl. **8**, 024007 (2017).

[22] M. Reindl, D. Huber, C. Schimpf, S. F. C. da Silva, M. B. Rota, H. Huang, V. Zwiller, K. D. Jöns, A. Rastelli, and R. Trotta, All-photonic quantum teleportation using on-demand solid-state quantum emitters, Sci. Adv. **4**, eaau1255 (2018).

[23] N. I. Cade, H. Gotoh, H. Kamada, H. Nakano, S. Anantathanasarn, and R. Nötzel, Optical characteristics of single InAs/InGaAsP/InP(100) quantum dots emitting at 1.55 μm, Appl. Phys. Lett. **89**, 181113 (2006).

[24] M. Benyoucef, M. Yacob, J. P. Reithmaier, J. Kettler, and P. Michler, Telecom-wavelength (1.5 μm) single-photon emission from InP-based quantum dots, Appl. Phys. Lett. **103**, 162101 (2013).

[25] M. Paul, F. Olbrich, J. Höschele, S. Schreier, J. Kettler, S. L. Portalupi, M. Jetter, and P. Michler, Single-photon emission at 1.55μm from MOVPE-grown InAs quantum dots on InGaAs/GaAs metamorphic buffers, Appl. Phys. Lett. **111**, 033102 (2017).

[26] K. D. Zeuner, M. Paul, T. Lettner, C. Reuterskiöld Hedlund, L. Schweickert, S. Steinhauer, L. Yang, J. Zichi, M. Hammar, K. D. Jöns, and V. Zwiller, A stable wavelength-tunable triggered source of single photons and cascaded photon pairs at the telecom C-band, Appl. Phys. Lett. **112**, 173102 (2018).

[27] J. Skiba-Szymanska, R. M. Stevenson, C. Varnava, M. Felle, J. Huwer, T. Müller, A. J. Bennett, J. P. Lee, I. Farrer, A. B. Krysa, P. Spencer, L. E. Goff, D. A. Ritchie, J. Heffernan, and A. J. Shields, Universal Growth Scheme for Quantum Dots with Low Fine-Structure Splitting at Various Emission Wavelengths, Phys. Rev. Appl. **8**, 014013 (2017).

[28] F. Olbrich, J. Höschele, M. Müller, J. Kettler, S. Luca Portalupi, M. Paul, M. Jetter, and P. Michler, Polarization-entangled photons from an InGaAs-based quantum dot emitting in the telecom C-band, Appl. Phys. Lett. **111**, 133106 (2017).

[29] T. Müller, J. Skiba-Szymanska, A. B. Krysa, J. Huwer, M. Felle, M. Anderson, R. M. Stevenson, J. Heffernan, D. A. Ritchie, and A. J. Shields, A quantum light-emitting diode for the standard telecom window around 1,550 nm, Nat. Commun. **9**, 862 (2018).

[30] C. Nawrath, F. Olbrich, M. Paul, S. L. Portalupi, M. Jetter, and P. Michler, Coherence and indistinguishability of highly pure single photons from non-resonantly and resonantly excited telecom C-band quantum dots, Appl. Phys. Lett. **115**, 023103 (2019).

[31] M. Anderson, T. Müller, J. Huwer, J. Skiba-Szymanska, A. Krysa, R. Stevenson, J. Heffernan, D. Ritchie, and A. Shields, Quantum teleportation using highly coherent emission from telecom C-band quantum dots, npj Quantum Inf. **6**, 14 (2020).

[32] A. Boaron, G. Boso, D. Rusca, C. Vulliez, C. Autebert, M. Caloz, M. Perrenoud, G. Gras, F. Bussières, M.-J. Li, D. Nolan, A. Martin, and H. Zbinden, Secure Quantum Key Distribution over 421 km of Optical Fiber, Phys. Rev. Lett. **121**, 190502 (2018).

[33] J. Zhang, J. S. Wildmann, F. Ding, R. Trotta, Y. Huo, E. Zallo, D. Huber, A. Rastelli, and O. G. Schmidt, High yield and ultrafast sources of electrically triggered entangled-photon pairs based on strain-tunable quantum dots, Nat. Commun. **6**, 10067 (2015).

[34] J. Brendel, N. Gisin, W. Tittel, and H. Zbinden, Pulsed Energy-Time Entangled Twin-Photon Source for Quantum Communication, Phys. Rev. Lett. **82**, 2594 (1999).

[35] J. F. Dynes, H. Takesue, Z. L. Yuan, A. W. Sharpe, K. Harada, T. Honjo, H. Kamada, O. Tadanaga, Y. Nishida, M. Asobe, and A. J. Shields, Efficient entanglement distribution over 200 kilometers, Opt. Express **17**, 11440 (2009).

[36] J. P. Lee, L. M. Wells, B. Villa, S. Kalliakos, R. M. Stevenson, D. J. P. Ellis, I. Farrer, D. A. Ritchie, A. J. Bennett, and A. J. Shields, Controllable Photonic Time-Bin Qubits from a Quantum Dot, Phys. Rev. X **8**, 021078 (2018).

[37] C. Simon and J.-P. Poizat, Creating Single Time-Bin-Entangled Photon Pairs, Phys. Rev. Lett. **94**, 030502 (2005).

[38] P. K. Pathak and S. Hughes, Coherent generation of time-bin entangled photon pairs using the biexciton cascade and cavity-assisted piecewise adiabatic passage, Phys. Rev. B **83**, 245301 (2011).

[39] H. Jayakumar, A. Predojević, T. Kauten, T. Huber, G. S. Solomon, and G. Weihs, Time-bin entangled photons from a quantum dot, Nat. Commun. **5**, 4251 (2014).

[40] T. Huber, L. Ostermann, M. Prilmüller, G. S. Solomon, H. Ritsch, G. Weihs, and A. Predojević, Coherence and degree of time-bin entanglement from quantum dots, Phys. Rev. B **93**, 201301(R) (2016).

[41] K. Sanaka, K. Kawahara, and T. Kuga, Experimental probabilistic manipulation of down-converted photon pairs using unbalanced interferometers, Phys. Rev. A **66**, 040301(R) (2002).

[42] M. A. M. Versteegh, M. E. Reimer, A. A. van den Berg, G. Juska, V. Dimastrodonato, A. Gocalinska, E. Pelucchi, and V. Zwiller, Single pairs of time-bin-entangled photons, Phys. Rev. A **92**, 033802 (2015).

[43] K. D. Jöns, L. Schweickert, M. A. M. Versteegh, D. Dalacu, P. J. Poole, A. Gulinatti, A. Giudice, V. Zwiller, and M. E. Reimer, Bright nanoscale source of deterministic entangled photon pairs violating Bell's inequality, Sci. Rep. **7**, 1700 (2017).

[44] P. Michler, *Single Semiconductor Quantum Dots*, Nano-Science and Technology (Springer-Verlag, Berlin, 2009).

[45] D. F. V. James, P. G. Kwiat, W. J. Munro, and A. G. White, Measurement of qubits, Phys. Rev. A **64**, 052312 (2001).

[46] B. J. Metcalf, J. B. Spring, P. C. Humphreys, N. Thomas-Peter, M. Barbieri, W. S. Kolthammer, X.-M. Jin, N. K. Langford, D. Kundys, J. C. Gates, B. J. Smith, P. G. R. Smith, and I. A. Walmsley, Quantum teleportation on a photonic chip, Nat. Photonics **8**, 770 (2014).

[47] J. M. Gérard, B. Sermage, B. Gayral, B. Legrand, E. Costard, and V. Thierry-Mieg, Enhanced Spontaneous Emission by Quantum Boxes in a Monolithic Optical Microcavity, Phys. Rev. Lett. **81**, 1110 (1998).

[48] A. J. Bennett, J. P. Lee, D. J. P. Ellis, T. Meany, E. Murray, F. F. Floether, J. P. Griffths, I. Farrer, D. A. Ritchie, and A. J. Shields, Cavity-enhanced coherent light scattering from a quantum dot, Sci. Adv. **2**, e1501256 (2016).